Journal of Electrical and Electronic Engineering
2022; 10(4): 142-148
http://www.sciencepublishinggroup.com/j/jeee
doi: 10.11648/j.jeee.20221004.12
ISSN: 2329-1613 (Print); ISSN: 2329-1605 (Online)

Fiber Fuse Simulation in Dispersion-Shifted Fibers

Yoshito Shuto

Ofra Project, Iruma, Japan

Email address:
ofra@tuba.ocn.ne.jp

To cite this article:
Yoshito Shuto. Fiber Fuse Simulation in Dispersion-Shifted Fibers. *Journal of Electrical and Electronic Engineering*. Vol. 10, No. 4, 2022, pp. 142-148. doi: 10.11648/j.jeee.20221004.12

Received: July 10, 2022; **Accepted**: July 22, 2022; **Published**: July 29, 2022

Abstract: Silica-based optical fibers are the most important transmission medium for long-distance and large-capacity optical communication systems. The most distinguished feature of optical fiber is its low loss characteristics. A single-mode optical fiber (SMF) exhibits a very low transmission loss (0.142 dB/km) at 1.55 μm. Together with such low loss characteristics, zero chromatic dispersion near 1.55 μm is required for high capacity signal transmission. The zero-dispersion wavelength of optical fibers can be shifted to the vicinity of 1.55 μm by the mutual cancellation of material dispersion and waveguide dispersion. Such fibers are called dispersion-shifted fibers (DSFs). The unsteady-state thermal conduction process in several DSFs was studied theoretically by the explicit finite-difference method using the thermochemical SiO_x production model. The calculated threshold power and velocity of fiber fuse propagation in a step-index SMF were in fair agreement with the experimental values observed at 1.55 μm. It was found that the calculated threshold powers were proportional to the effective cross sectional areas of several DSFs and there is a linear relationship between the threshold powers and the mode-field diameters in the range of up to 2 W. These results were in fair agreement with the experimental results observed at 1.55 μm.

Keywords: Fiber Fuse Phenomenon, Dispersion-Shifted Fibers, Finite-Difference Technique

1. Introduction

Silica-based optical fibers are the most important transmission medium for long-distance and large-capacity optical communication systems. The most distinguished feature of optical fiber is its low loss characteristics. A very low loss single-mode fiber (SMF) with a minimum loss of 0.20 dB/km at a wavelength (λ_0) of 1.55 μm was reported in 1979 [1], and the lower transmission loss of 0.154 dB/km at λ_0 = 1.55 μm was achieved in 1986 [2], and the lowest transmission loss of 0.142 dB/km at this wavelength was achieved in 2018 [3].

Together with such low loss characteristics, zero chromatic dispersion near λ_0 = 1.55 μm is required for high capacity signal transmission. Chromatic dispersion in a SMF is the sum of material dispersion and waveguide dispersion. A silica-based SMF exhibits zero material dispersion in the vicinity of 1.3 μm [4, 5]. The waveguide dispersion can be controlled by the proper choice of the waveguide parameters, while the material dispersion is almost independent of these parameters. Therefore, the zero-dispersion wavelength λ_{cd}^0, at which the chromatic dispersion becomes zero, can also be controlled by changing the core diameter, doping concentration, and relative refractive-index difference Δ [6-12]. λ_{cd}^0 of SMFs can be shifted to the vicinity of 1.55 μm by the mutual cancellation of material dispersion and waveguide dispersion [6, 7, 11]. Such fibers are called dispersion-shifted fibers (DSFs).

In this article, the unsteady-state thermal conduction process in dispersion-shifted fibers was investigated theoretically with the explicit finite-difference method using the thermochemical SiO_x production model [13].

2. Characteristics of Dispersion-Shifted Fibers

The waveguide (and also chromatic) dispersion can be tailored by controlling the core size and shape, which is related with the refractive-index profile in the fiber [6]. The DSFs can be classified as single-clad or multi-clad fibers.

2.1. Single-Clad Fibers

The single-clad fiber includes a triangular-shape fiber (TriSF) [14, 15]. The refractive-index profile of the TriSF is shown in Figure 1.

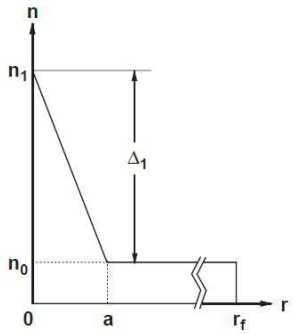

Figure 1. *Refractive-index profile of TriSF.*

In this figure, r_f is the fiber radius, a is the core radius, and n_1 and n_0 are the maximum refractive-index in the core and the cladding refractive-index, respectively. Δ_1 is the relative refractive-index difference between n_1 and n_0.

The parameters of two TriSFs are shown in Table 1, together with a conventional step-index SMF.

Table 1. *Parameters of step-index SMF and TriSFs.*

Parameters	Unit	SMF	TriSF1	TriSF2
Δ_1	%	0.30	0.548	0.80
a	μm	4.6	2.7	2.7
λ_{cd}^0	μm	1.31	1.45	1.55
A_{eff}	μm^2	93.11	287.52	88.23

In this table, A_{eff} is the effective cross sectional area at 1.55 μm, which was estimated with the finite element method (FEM) [16].

Chromatic dispersion in the 1.0-1.7-μm spectral region for the step-index SMF and the TriSFs were calculated by using the FEM program. The calculated results are shown in Figure 2.

It is clear that zero chromatic dispersion of TriSF1 and TriSF2 occurs at 1.45 and 1.55 μm, which is longer than the zero-dispersion wavelength λ_{cd}^0 (= 1.31 μm) of the SMF.

However, the TriSFs have one serious disadvantage. It is well known that the LP_{11} mode cutoff wavelength in them is shorter than 1 μm [14, 15], which is too far from the operating wavelength of 1.55 μm. Accordingly, the spread of the modal field into the cladding is quite large, as shown in the A_{eff} value (= 287 μm^2) of TriSF1 (see Table 1), and therefore, the TriSFs exhibit excessive sensitivity to bend-induced losses.

The spread of the field in the cladding can be reduced by introducing extra cladding layers around the core. Such multi-clad fiber is described below.

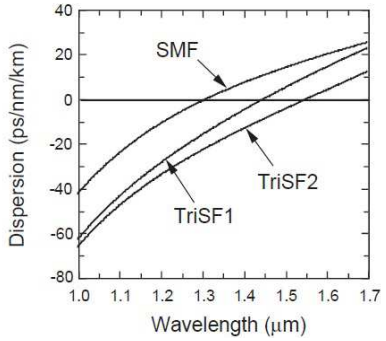

Figure 2. *Chromatic dispersion of step-index SMF and TriSFs.*

2.2. Multi-clad Fibers

The multi-clad fibers include the *W*-type fiber with a narrow depressed cladding layer [17-19], the segmented-core fiber [20, 21], and the dual-shape core fiber (DSCF) [22-24]. Among these core/cladding designs, the dual-shape core design has been widely used in the conventional DSF and in the non-zero DSF (NZ-DSF).

As the DSF and NZ-DSF exhibit higher Raman gain efficiencies than those of the step-index SMFs [25, 26], these fibers have been used in long-haul transmission systems employing distributed Raman amplifiers [25, 27-32].

In contrast, a broad dispersion compensation fiber (BDCF) [33, 34] with large negative chromatic dispersion in the 1.55 μm region has also been employed in the Raman amplifiers [35-39].

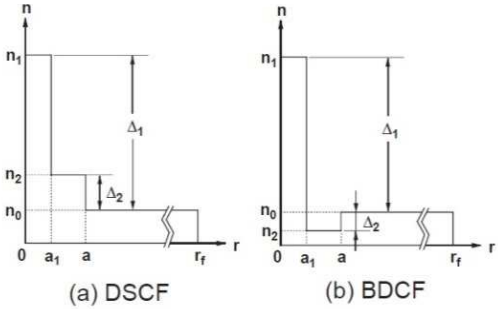

Figure 3. *Refractive-index profiles of a DSCF and BDCF.*

The refractive-index profile of the DSCF and BDCF are shown in Figure 3.

In this figure, a_1 and a are the inner and outer core radii, and n_1 and n_2 are the refractive indices in the inner and outer core, respectively. Δ_2 is the relative refractive-index difference between n_2 and n_0.

The BDCF is a kind of *W*-type fiber with a depressed cladding layer. In this fiber, n_2 is smaller than n_0, and therefore, Δ_2 takes a negative value.

The parameters of three types of DSCFs and the BDCF are shown in Table 2.

Table 2. *Parameters of DSCFs and BDCF.*

Parameters	Unit	NZ(+)- DSF	DSF	NZ(-)- DSF	BDCF
Δ_1	%	0.62	0.74	0.90	1.90
Δ_2	%	0.124	0.148	0.180	-0.35
a	μm	3.6	3.2	3.0	4.44
a_1	μm	1.8	1.6	1.5	1.4
λ_{cd}^0	μm	1.50	1.55	1.61	-
A_{eff}	μm^2	79.30	70.25	54.18	16.60

Chromatic dispersions in the 1.3-1.7-μm spectral region for the step-index SMF and the DSCFs are shown in Figure 4.

It is clear that zero chromatic dispersion of the DSF occurs between those of NZ(+)-DSF and NZ(-)-DSF, and the zero-dispersion wavelengths λ_{cd}^0 of these fibers are longer than that of the SMF.

Chromatic dispersions in the 1.3-1.7-μm spectral region for the step-index SMF and the BDCF are shown in Figure 5.

It is clear that the BDCF exhibits large negative chromatic

dispersion (about -110 ps/km·nm) and dispersion slope (about -0.443 ps/km/nm^2) at 1.55 μm. This fiber can compensate the dispersion and dispersion slope of the conventional step-index SMF over the optical bandwidth of more than 100 nm [35, 37, 40].

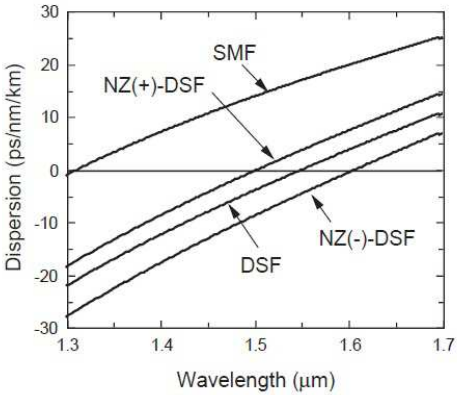

Figure 4. *Chromatic dispersion of step-index SMF and DSCFs.*

In the next section, the results of some numerical calculations related to the thermal conduction process in various DSFs are described.

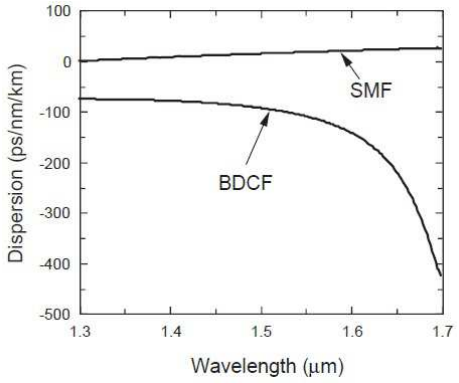

Figure 5. *Chromatic dispersion of step-index SMF and BDCF.*

3. Fiber Fuse Calculation in DSFs

The first fiber fuse experiments were conducted in two TriSFs (TriSF1 and TriSF2 in Table 1) by Kashyap and co-workers, together with a step-index SMF at λ_0 = 0.514 and 1.064 μm [41-43]. We reported that the propagation velocities of fiber fuse in a step-index SMF and TriSFs, which were theoretically estimated at λ_0 = 1.064 μm, were in fairly good agreement with the experimentally determined values [44, 45]. Several experiments had also been carried out on the fiber fuse phenomenon in the DSFs at λ_0 = 1.064, 1.467, and 1.55 μm [46-53].

In this section, we do some numerical calculations related to the thermal conduction process in the DSF at λ_0 = 1.55 μm.

We assume that the DSF is in an atmosphere of $T = T_a$ and r_f of the DSF is 62.5 μm. We also assume that part of the core layer is heated and has a length of ΔL (= 40 μm) and a temperature of T_c^0 (> T_a) (see Figure 6).

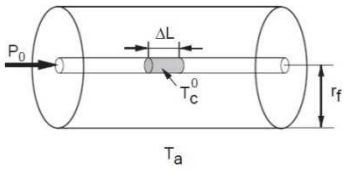

Figure 6. *Schematic view of hot zone in core layer.*

In the heating zone (called the "hot zone") shown in Figure 6, an absorption coefficient α is larger than in the other parts of the core because of its high temperature T_c^0 (> T_a). Thus, as the light propagates along the positive direction (away from the light source) in this zone, a considerable amount of heat is produced by light absorption.

The heat conduction equation for the temperature field T (r, z, t) in the DSF is given by [54]

$$\rho C_p \frac{\partial T}{\partial t} = k\left(\frac{\partial^2 T}{\partial r^2} + \frac{1}{r}\frac{\partial T}{\partial r} + \frac{\partial^2 T}{\partial z^2}\right) + \dot{Q} \tag{1}$$

where ρ, C_p, and k are the density, specific heat, and thermal conductivity of the fiber, respectively.

The last term $\dot{Q}$ in Eq. (1) represents the heat source caused by light absorption, which is required only for the hot zone in the fiber core. $\dot{Q}$ can be given by

$$\dot{Q} = \alpha I \tag{2}$$

where I is the optical power intensity of the core layer.

We assume that the I value is given by dividing the optical power by the effective cross sectional area of the DSF. That is, I is given by

$$I = \frac{P_0}{A_{eff}} \tag{3}$$

where P_0 is the incident optical power.

We investigated the core center temperature distribution in the longitudinal direction of the SMF and DSF after the incidence of a laser power P_0 of up to 2 W. The calculation by the finite-difference method followed the procedure described in the literature [13]. In the calculation, the time interval δt was set to 10 ns, the step size along the r axis δr to r_f/14, and the step size along the z axis δz to 20 μm, respectively, and it was assumed that T_c^0 = 2,923 K and T_a = 298 K.

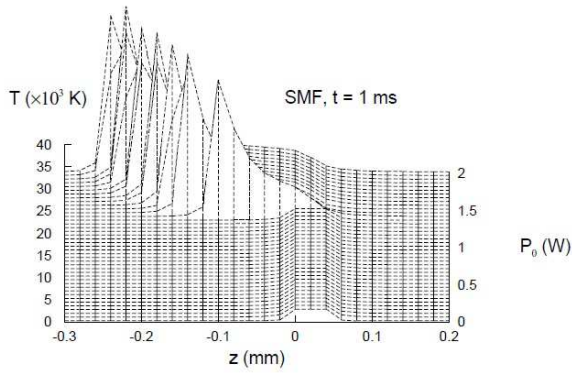

Figure 7. *Core center temperature distribution in the longitudinal direction of the SMF after 1 ms when P_0 = 0-2 W and λ_0 = 1.55 μm.*

We estimated the change in the temperature T (0, z) at the core center (r = 0 μm) in the SMF and DSF at t = 1 ms after the incidence of laser light with λ_0 = 1.55 μm and initial power P_0 = 0-2 W. The calculated changes in the temperature at the core center position are shown in Figures 7 and 8.

When the power of the light entering the SMF increases from 1.3 W to 1.4 W, the peak temperature rises from 2,923 to 34,000 K, and thereafter, propagation behavior was observed in the -z direction with increasing P_0, as shown in Figure 7. The characteristic P_0 value of 1.4 W is the threshold power P_{th} of the SMF. This value is close to the experimental P_{th} value of 1.39 W [53]. The P_{th} of the DSF is determined as 1.05 W in the same manner as the SMF, as shown in Figure 8.

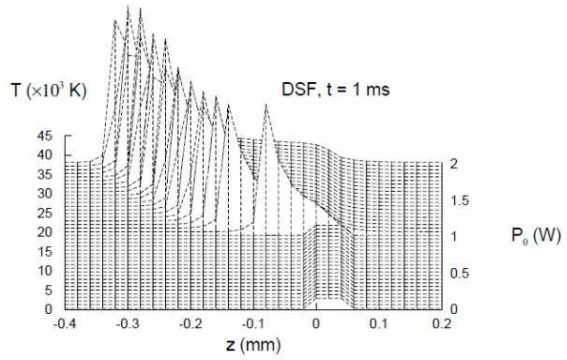

Figure 8. *Core center temperature distribution in the longitudinal direction of the DSF after 1 ms when P_0 = 0-2 W and λ_0 = 1.55 μm.*

Furthermore, the change in the temperature T (0, z) at the core center (r = 0 μm) in the TriSF1 was investigated at t = 1 ms after the incidence of a laser power P_0 of up to 6 W. The calculated change in the temperature at the core center position is shown in Figure 9. As shown in this figure, when the power of the light entering the TriSF1 increases from 4.2 W to 4.3 W, the peak temperature rises from 2,923 to 34,000 K, and thereafter propagation behavior was observed in the -z direction with increasing P_0. The P_{th} of the TriSF1 is determined to 4.28 W. This value is three or four times larger than that of the SMF (1.40 W) or DSF (1.05 W) because the A_{eff} value of the TriSF1 is larger than that of the SMF or DSF.

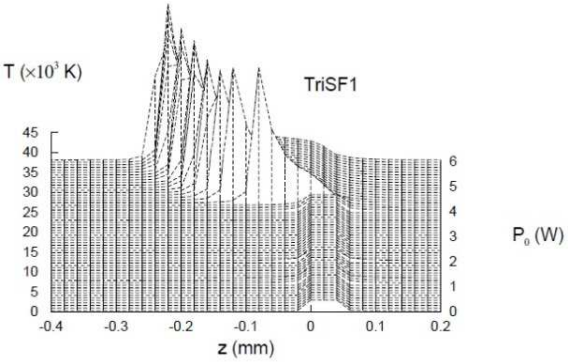

Figure 9. *Core center temperature distribution in the longitudinal direction of the TriSF1 after 1 ms when P_0 = 0-6 W and λ_0 = 1.55 μm.*

Next, the temperature field of the core center of the SMF was estimated along the z direction at t = 1 ms and 10 ms after the incidence of laser light with P_0 = 2 W and λ_0 = 1.55 μm.

The calculated results are shown in Figure 10.

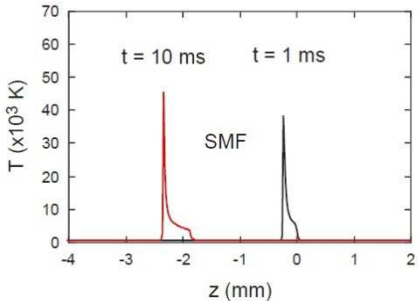

Figure 10. *Temperature fields of the core center of SMF after 1 and 10 ms when P_0 = 2 W and λ_0 = 1.55 μm.*

As shown in Figure 10, the core center temperature near the end of the hot zone (z = -0.24 mm) changes abruptly to a high value of about 3.5 × 10^4 K after 1 ms. This rapid rise in the temperature initiates the fiber fuse propagation. After 10 ms, the high-temperature front in the core layer reaches a z value of -2.62 mm. The average propagation velocity V_f is estimated to be 0.26 m/s using these data. This V_f is close to the value (~0.32 m/s) measured by Abedin and Nakazawa [53].

The parameters and P_{th} values of various fibers are shown in Table 3.

Table 3. *Parameters and P_{th} values of various fibers.*

Fibers	A_{eff} (μm²)	ω (μm)	P_{th} (W)
SMF	93.11	5.60	1.40
TriSF1	287.52	9.85	4.28
TriSF2	88.23	5.45	1.32
NZ(+)-DSF	79.30	5.17	1.19
DSF	70.25	4.87	1.05
NZ(-)-DSF	54.18	4.27	0.82
BDCF	16.60	2.37	0.26

In this table, ω is the mode field radius at λ_0 = 1.55 μm. ω is approximately defined as

$$\omega = \sqrt{\frac{A_{eff}}{k\pi}} \quad (4)$$

where k (= 0.944) is the correction factor of A_{eff} and ω [55].

We examined the A_{eff} dependence of the P_{th} values at λ_0 = 1.55 μm. The results are shown in Figure 11.

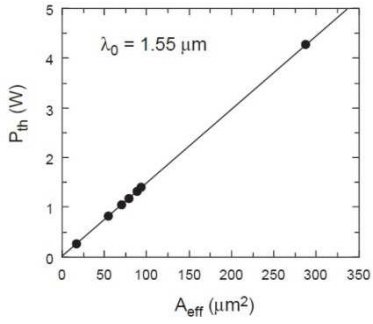

Figure 11. *Effective cross-sectional area dependence of the threshold powers at λ_0 = 1.55 μm.*

As shown in Figure 11, the P_{th} values are proportional to the A_{eff} values.

On the other hand, several researchers reported that the P_{th} value is linearly proportional to the mode-field diameter MFD (= 2ω) at λ_0 = 1.55 μm [51, 52].

Figure 12 shows the MFD dependence of the P_{th} value of various fibers.

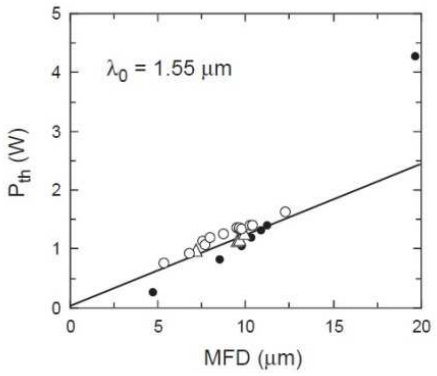

Figure 12. *MFD dependence of the threshold powers at λ_0 = 1.55 μm. The closed circles are the calculated values, the open circles are the data reported by Takenaga et al. [51], and the open triangles are the data reported by Takara et al. [52].*

It was found that there is a linear relationship between the P_{th} values and MFD value in the range of P_{th} < 2 W. This result is the same as that observed by Takenaga et al. [51] and Takara et al. [52], as shown in Figure 12.

From these results, it can be concluded that expanding the MFD and increasing the A_{eff} is an effective way to raise the power threshold for fiber fuse propagation in the dispersion-shifted fibers.

4. Conclusion

Together with such low loss characteristics, zero chromatic dispersion near 1.55 μm is required for high capacity signal transmission. The zero-dispersion wavelength of optical fibers can be shifted to the vicinity of 1.55 μm by the mutual cancellation of material dispersion and waveguide dispersion. Such fibers are called dispersion-shifted fibers (DSFs). The unsteady-state thermal conduction process in several DSFs was studied theoretically by the explicit finite-difference method using the thermochemical SiO_x production model. The calculated threshold power and velocity of fiber fuse propagation in a step-index SMF were in fair agreement with the experimental values observed at 1.55 μm. It was found that the calculated threshold powers were proportional to the effective cross sectional areas of several DSFs and there is a linear relationship between the threshold powers and the mode-field diameters in the range of up to 2 W. These results were in fair agreement with the experimental results observed at 1.55 μm.

Acknowledgements

The author is especially indebted to Dr. Katsunari Okamoto (Okamoto Laboratory) for his support with the FEM calculation program for optical fibers.

References

[1] Miya T., Terunuma Y., Hosaka T., and Miyashita T. (1979). Ultimate low-loss single-mode fibre at 1.55 μm. Electron. Lett., 15 (4), 106-108.

[2] Kanamori H., Yokota H., Tanaka G., Watanabe M., Ishiguro Y., Yoshida I., Kakii T., Itoh S., Asano Y., and Tanaka S. (1986). Transmission characteristics and reliability of pure-silica-core single-mode fibers. IEEEE J. Lightwave Technol., 4 (8), 1144-1150.

[3] Tamura Y., Sakuma H., Morita K., Suzuki M., Yamamoto Y., Shimada K., Honma Y., Sohma K., Fujii T., and Hasegawa T. (2018). The first 0.14-dB/km loss optical fiber and its impact on submarine transmission. IEEE J. Lightwave Technol., 36 (1), 44-49.

[4] Payne D. N. and Gambling W. A. (1975). Zero material dispersion in optical fibres. Electron. Lett., 11 (4), 176-178.

[5] South C. R. (1979). Total dispersion in step-index monomode fibres. Electron. Lett., 15 (13), 394-395.

[6] Cohen L. G., Lin C., and French W. G. (1979). Tailoring zero chromatic dispersion into the 1.5-1.6 μm low-loss spectral region of single-mode fibres. Electron. Lett., 15 (12), 334-335.

[7] White K. I. and Nelson B. P. (1979). Zero total dispersion in step-index monomode fibres at 1.30 and 1.55 μm. Electron. Lett., 15 (13), 396-397.

[8] Gambling W. A., Matsumara H., and Ragdale C. M. (1979). Zero total dispersion in graded-index single-mode fibres. Electron. Lett., 15 (13), 474-476.

[9] Tsuchiya H. and Imoto N. (1979). Dispersion-free single-mode fibre in 1.5 μm wavelength region. Electron. Lett., 15 (13), 476-478.

[10] Jeunhomme L. (1979). Dispersion minimisation in single-mode fibres between 1.3 μm and 1.7 μm. Electron. Lett., 15 (13), 478-479.

[11] Okamoto K., Edahiro T., Kawana A., and Miya T. (1979). Dispersion minimisation in single-mode fibres over a wide spectral range. Electron. Lett., 15 (22), 729-731.

[12] Jürgensen K. (1979). Dispersion minimum of monomode fibres. Appl. Opt., 18 (8), 1259-1261.

[13] Shuto Y. (2014). Heat conduction modeling of fiber fuse in single-mode optical fibers. J. Photonics, 2014, 645207.

[14] Saifi M. A., Jang S. J., Cohen L. G., and Stone J. (1982). Triangular-profile single-mode fiber. Opt. Lett., 7 (1), 43-45.

[15] Ainslie B. J., Beales K. J., Cooper D. M., Day C. R., and Rush J. D. (1982). Monomode fibre with ultra-low loss and minimum dispersion at 1.55 μm. Electron. Lett., 18 (19), 842-844.

[16] Okamoto K. (2022). Fundamentals of Optical Waveguides. 3rd Ed. Chap. 6, Academic Press, New York.

[17] Kawakami S. and Nishida S. (1974). Anomalous dispersion of new doubly clad optical fibre. Electron. Lett., 10 (4), 38-40.

[18] Kawakami S. and Nishida S. (1974). Characteristics of a doubly clad optical fiber with a low-index inner cladding. IEEE J. Quantum Electron., QE-10 (12), 879-887.

[19] Miya T., Okamoto K., Ohmori Y., and Sasaki Y. (1981). Fabrication of low dispersion single-mode fibers over a wide spectral range. IEEE J. Quantum Electron., QE-17 (6), 858-861.

[20] Bhagavatula V. A., Spotz M. S., Love W. F., and Keck D. B. (1983). Segmented-core single-mode fibres with low loss and low dispersion. Electron. Lett., 19 (8), 317-318.

[21] Bhagavatula V. A., Spotz M. S., and Love W. F. (1984). Dispersion-shifted segmented-core single-mode fibers. Opt. Lett., 9 (5), 186-188.

[22] Kubota M., Furuya K., and Suematsu Y. (1980). Random-bend loss-evaluation in single-mode optical fiber with various index profiles. Trans. IECE Japan, E63 (10), 723-730.

[23] Kuwaki N., Ohashi M., Tanaka C., and Uesugi N. (1985). Dispersion-shifted convex-index single-mode fibres. Electron. Lett., 21 (25), 1186-1187.

[24] Kuwaki N., Ohashi M., Tanaka C., Uesugi N., Seikai S., and Negishi Y. (1987). Characteristics of dispersion-shifted dual shape core single-mode fibers. IEEE J. Lightwave Technol., LT-5 (6), 792-797.

[25] Namiki S. and Emori Y. (2001). Ultrabroad-band Raman amplifiers pumped and gain-equalized by wavelength-division-multiplexed high-power laser diodes. IEEE J. Selected Topics Quantum Electron., 7 (1), 3-16.

[26] Bromage J. (2004). Raman amplification for fiber communication systems. IEEE J. Lightwave Technol., 22 (1), 79-93.

[27] Hansen P. B., Eskildsen L., Grubb S. G., Stentz A. J., Strasser T. A., Judkins J., DeMarco J. J., Pedrazzani R., and DiGiovanni D. J. (1997). Capacity upgrades of transmission systems by Raman amplification. IEEE Photon. Technol. Lett., 9 (2), 262-264.

[28] Suzuki H., Kani J., Masuda H., Tachio N., Iwatsuki K., Tada Y., and Sumida M. (2000). 1-Tb/s (100 × 10 Gb/s) super-dense WDM transmission with 25-GHz channel spacing in the zero-dispersion region employing distributed Raman amplification technology. IEEE Photon. Technol. Lett., 12 (7), 903-905.

[29] Sobe M. and Yano Y. (2002). Automatic pump power adjustment for gain-flattened multi-wavelength pumped Raman amplifier. Optical Fiber Commun. Conf. (OFC 2002), TuJ5.

[30] Fludger C. R. S., Handerek V., Jolley N., and Mears R. J. (2002). Novel ultra-broadband high performance distributed Raman amplifier employing pump modulation. Optical Fiber Commun. Conf. (OFC 2002), WB4.

[31] Leng L., Stulz S., Zhu B., Nelson L. E., Edvold B., Gruner-Nielsen L., Radic S., Centanni J., and Gnauck A. (2003). 1.6-Tb/s (160 × 10.7 Gb/s) transmission over 4000 km of nonzero dispersion fiber at 25-GHz channel spacing. IEEE Photon. Technol. Lett., 15 (8), 1153-1155.

[32] Zhu B., Doerr C. R., Gaarde P., Nelson L. E., Stulz S., Stulz L., and Gruner-Nielsen L. (2003). Broad bandwidth seamless transmission of 3.56 Tbit/s over 40 × 100 km of NZDF fibre using CSRZ-DPSK format. Electron. Lett., 39 (21), 1528-1530.

[33] Grüner-Nielsen L., Knudsen S. N., Edvold B., Veng T., Magnussen D., Larsen C. C., and Damsgaard H. (2000). Dispersion compensating fibers. Opt. Fiber Technol., 6, 164-180.

[34] Grüner-Nielsen L., Wandel M., Kristensen P., Jorgensen C., Jorgensen L. V., Edvold B., Pálsdóttir B., and Jakobsen D. (2005). Dispersion-compensating fibers. IEEE J. Lightwave Technol., 23 (11), 3566-3579.

[35] Emori Y., Tanaka K., and Namiki S. (1999). 100 nm bandwidth flat-gain Raman amplifiers pumped and gain-equalised by 12-wavelength-channel WDM laser diode unit. Electron. Lett., 35 (16), 1355-1356.

[36] Tsuzaki T., Kakui M., Hirano M., Onishi M., and Nishimura M. (2001). Broadband discrete fiber Raman amplifier with high differential gain operating over 1.65 μm-band. Optical Fiber Commun. Conf. (OFC 2001), MA3.

[37] Miyamoto T., Tsuzaki T., Okuno T., Kakui M., Hirano M., Onishi M., and Shigematsu M. (2002). Raman amplification over 100 nm-bandwidth with dispersion and dispersion slope compensation for conventional single mode fiber. Optical Fiber Commun. Conf. (OFC 2002), TuJ7.

[38] Yam S. S-H., An F-T., Hu E. S-T., Marhic M. E., Sakamoto T., Kazovsky L. G., and Asakawa Y. (2002). Gain-clamped S-band discrete Raman amplifier. Optical Fiber Commun. Conf. (OFC 2002), ThB4.

[39] Kotanigawa T., Matsuda T., and Naka A. (2004). Unstable Raman amplification due to Brillouin scattering and its suppression for 40 Gb/s WDM transmission. Optical Fiber Commun. Conf. (OFC 2004), WB2.

[40] Hirano M., Tada A., Kato T., Onishi M., Makio Y., and Nishimura M. (2001). Dispersion compensating fiber over 140 nm-bandwidth. 27th Eur. Conf. Optical Commun. (ECOC 2001), Th. M. 1.4.

[41] Kashyap R. (1988). Self-propelled self-focusing damage in optical fibres. Lasers'87: Proc. Xth Int. Conf. Lasers and Applications, 859-866, STS Press, McLean.

[42] Kashyap R., Sayles A., and Cornwell G. F. (1996). Heat flow modeling and visualisation of catastrophic self-propagating damage in single-mode optical fibres at low powers. Proc. Soc. Photo-Opt. Instrum. Eng., 2966, 586-591.

[43] Kashyap R. (2003). High average power effects in optical fibres and devices. Proc. Soc. Photo-Opt. Instrum. Eng., 4940, 108-117.

[44] Shuto Y., Yanagi S., Asakawa S., Kobayashi M., and Nagase R. (2004). Fiber fuse phenomenon in step-index single-mode optical fibers. IEEE J. Quantum Electron., 40 (8), 1113-1121.

[45] Shuto Y., Yanagi S., Asakawa S., Kobayashi M., and Nagase R. (2006). Fiber fuse phenomenon in triangular-profile single-mode optical fibers. IEEE J. Lightwave Technol., 24 (2), 846-852.

[46] Davis D. D., Mettler S. C., and DiGiovani D. J. (1995). Experimental data on the fiber fuse. Proc. Soc. Photo-Opt. Instrum. Eng., 2714, 202-210.

[47] Davis D. D., Mettler S. C., and DiGiovani D. J. (1996). A comparative evaluation of fiber fuse models. Proc. Soc. Photo-Opt. Instrum. Eng., 2966, 592-606.

[48] Yanagi S., Asakawa S., and Nagase R. (2002). Characteristics of fibre-optic connector at high-power optical incidence. Electron. Lett., 38 (17), 977-978.

[49] Seo K., Nishimura N., Shiino M., Yuguchi R., and Sasaki H. (2003). Evaluation of high-power endurance in optical fiber links. Furukawa Rev., 24, 17-22.

[50] Nishimura N., Seo K., Shiino M., and Shiba T. (2003). Study of high-power endurance characteristics in optical fiber link. Technical Digest of Opt. Amplifiers and Their Applications, 94-97.

[51] Takenaga K., Omori S., Goto R., Tanigawa S., Matsuo S., and Himeno K. (2008). Evaluation of high-power endurance of bend-insensitive fibers. Technical Digest of Opt. Fiber Conf. (OFC 2008), 370-372.

[52] Takara H., Masuda H., Kanbara H., Abe Y., Miyamoto Y., Nagase R., Morioka T., Matsuoka S., Shimizu M., and Hagimoto K. (2009). Evaluation of fiber fuse characteristics of hole-assisted fiber for high power optical transmission systems. Technical Digest of European Conf. Opt. Commun. (ECOC 2009), 918-919.

[53] Abedin K. S. and Nakazawa M. (2010). Real time monitoring of a fiber fuse using an optical time-domain reflectometer. Opt. Express, 18 (20), 21315-21321.

[54] Carslaw H. S. and Jaeger J. C. (1959). Conduction of Heat in Solids. 2nd Ed. Chap. 13, Oxford University Press, Inc., Oxford.

[55] Namihira Y. (1994). Relationship between nonlinear effective area and modefield diameter for dispersion shifted fibres. Electron. Lett., 30 (3), 262-264.